Available online at www.sciencedirect.com
ScienceDirect
International Journal of Heat and Mass Transfer 51 (2008) 2455–2461
International Journal of HEAT and MASS TRANSFER
www.elsevier.com/locate/ijhmt

Spreading and solidification of a highly undercooled $Y_3Al_5O_{12}$ droplet impinging on a substrate

K. Nagashio [a,*], K. Kodaira [b], K. Kuribayashi [a], T. Motegi [b]

[a] *Institute of Space and Astronautical Science (ISAS), Japan Aerospace Exploration Agency (JAXA), 3-1-1 Yoshinodai, Sagamihara, Kanagawa 229-8510, Japan*

[b] *Chiba Institute of Technology, 2-17-1 Tsudanuma, Narashino, Chiba 275-0016, Japan*

Received 14 February 2007; received in revised form 18 July 2007
Available online 27 September 2007

Abstract

Because of the containerless state, an in-flight droplet in thermal spray coating (TSC) has been presumed to experience a large undercooling prior to impact on a substrate. In the present investigation, using a $Y_3Al_5O_{12}$ (YAG) droplet as a model material for TSC, the spreading and solidification of the droplet impacted on a substrate were investigated over a wide range of undercoolings by means of both levitation and high-speed imaging techniques. The maximum spread of the droplets upon impact decreased with increasing undercoolings. The rebound of the droplets observed at high temperature also disappeared with increasing undercoolings. These results suggest that the spreading behavior and the final splat shape are strongly influenced by undercoolings because of their increase in viscosity.

Keywords: YAG; Undercooling; Spreading; Viscosity; Surface energy

1. Introduction

One of the practical techniques for thermal barrier coating (TBC) is thermal plasma spraying (TPS), in which small powders are melted, accelerated in a high-velocity gas stream at a high temperature, and then deposited on a substrate [1]. The elemental processes of TPS are the spreading, solidification and adhesion of a single droplet on a substrate. Quantitative understanding of these elemental processes, which has been highly desired for optimization of the TPS process, was prevented by its extreme severe conditions, such as the particle size of ~50 μm and the flight velocity of $\sim 10^2$–10^3 m/s. Recent progress in high-speed optical pyrometry has enabled direct detection of the impact behavior of the droplet [2–4]. The temperature data obtained on yttria-stabilized zirconia suggested that the droplet might experience undercooling prior to impacting the substrate [4]. Furthermore, numerical calculations predicted that the in-flight droplets, which are in a containerless state without an extrinsic heterogeneous nucleation site such as crucible wall, undercool deeply below the melting temperature [5]. Past model analyses of the TPS process [6,7] have included the impact velocity, surface energy and substrate temperature as experimental parameters controlling the spreading behavior, however, the effect of the undercooling has never been addressed despite its large influence on the spreading and solidification behavior.

Previously, the authors have studied the rapid solidification from the undercooled melt of the metallic material using an electromagnetic levitator (EML) [8]. In addition, the authors recently combined the EML apparatus with an infrared (IR) thermal imaging system to observe the solidification behavior of a silicon droplet impacted onto a silicon wafer. They reported that the final splat shape strongly depends on the undercooling of the droplet since the solidification rate in the undercooled melt was so high to prevent the droplet spreading [9,10]. In the TPS process, the large energy barrier for the formation of the critical

* Corresponding author. Tel.: +81 42 759 8264; fax: +81 42 759 8461.
E-mail address: nagashio@isas.jaxa.jp (K. Nagashio).

0017-9310/$ - see front matter © 2007 Elsevier Ltd. All rights reserved.
doi:10.1016/j.ijheatmasstransfer.2007.08.008

nucleus in oxide materials such as yttria-stabilized zirconia (YSZ) enhances the undercooling of the droplet not only in-flight but also at the impact on the substrate. On the other hand, the growth kinetics is much slower than that of metals. In this case, the viscosity of the undercooled droplet will considerably affect the spreading behavior.

Here, the maximum undercooling obtained for YAG is reported to be ~1000 K even for millimeter-size droplet [11], while those of typical TBC materials such as Al_2O_3 and YSZ are typically ~300–400 K where the increase in viscosity will not be so large. In case of particle size of ~50 μm, however, larger undercooling can be expected even for TBC materials. In the present study, $Y_3Al_5O_{12}$ (YAG) was used as a model sample to simulate the TSP process. The objective of this study is to elucidate the effects of the viscosity on the spreading and solidification behaviors of the droplet impinging on a substrate as a function of initial undercoolings.

2. Experimental procedure

The spherical YAG samples were prepared by melting the YAG powders using a CO_2 laser on a water-cooled copper hearth. The powders melted from the top became hemisphere shape due to the surface tension and this melting process was iterated several times, which resulted in spherical shape. The typical diameter and mass were ~2.5 and ~25 mg, respectively. The sample was levitated by a separative aerodynamic levitator (ADL), as shown in Fig. 1, in O_2 gas flow and melted completely by the CO_2 laser from the top. The surface temperature was monitored by a thermopile with broadband operating wavelength from 4.6 to 5.2 μm and a spot diameter of 2 mm. The droplet's undercooling was maintained by adjusting the CO_2 laser output. Finally, the ADL nozzle was separated toward either side as, simultaneously, the shutter of the CO_2 laser was closed and the levitation gas was stopped. Then, the droplet began freefall.

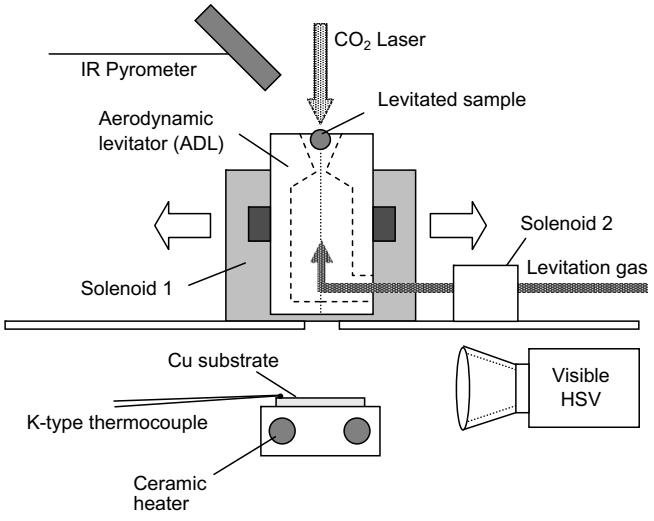

Fig. 1. Schematic diagram of aerodynamic levitator and imaging system.

In this study, the mirror-polished copper plate, 2 mm thick, was used as the substrate at two kinds of heating conditions of room temperature and 573 K. The copper substrate's wettability to the molten sample was increased by heating using two ceramic heaters. The substrate reached the predetermined temperature in ~30 min with a temperature distribution of ±3 K/cm. The distance from the levitated sample to the substrate was adjusted to 15 cm to yield a droplet impact velocity of approximately 1.7 m/s. The sequence of dropping, impacting, spreading and solidification of the droplet was monitored from the side of the substrate using a high-speed video camera (HSV) at 5 kHz for 128×80 pixels or at 1 kHz for 256×240 pixels. The experimental details are given elsewhere [12]. The spreading factor, D/d (the ratio of the splat diameter, D, to the initial droplet diameter, d), was measured by extracting the edge of the droplet in the HSV image.

3. Results

Fig. 2 shows the selected frames of HSV images taken at 1 kHz for droplets with different initial temperatures. The copper substrate was kept at room temperature. The time indicated in each image was set at 0 ms for one frame before impact. In the sample dropped at 2474 K (a), which is 260 K higher than the melting point ($T_M = 2213$ K), the droplet diameter reached its maximum at 2 ms and rebounded at ~6 ms. Finally, a small droplet necked off from the original one at 8 ms. The main droplet fell back at ~150 ms, rebounded again and disappeared from the screen. According to further frames, not shown here, the main droplet seemed to be semi-solid state at its second rebound. The contact angle at the droplet edge was always larger than 90°, indicating that the molten YAG is repelled from the copper substrate. In the sample dropped at 2070 K ($\Delta T = 143$ K), as shown in Fig. 2b, the spreading behavior was similar to that in (a), but the detachment of a small droplet did not occur. When the droplet rebounded, no solid was detected from the side view even though the quenched region was apparently observed at $t > 5$ ms. However, very recent study using a new HSV with the high-spatial resolution (1024×1024 at 5 kHz) confirmed that the solidification occurred only at the quenched surface. The thin solid layer was engulfed into the droplet during recoiling. On the other hand, in the sample dropped at 1418 K ($\Delta T = 795$ K) (c), the maximum splat diameter was considerably decreased. After the impact, the droplet stayed on the substrate and then solidified from the center position, which had been the edge at the maximum splat size. The temperature of the solid was higher than the undercooled droplet because of the latent heat release. The intensities for different samples cannot be compared as a function of temperature because the aperture for the optical lens of the HSV was individually optimized for each sample.

Although the HSV images taken at 1 kHz are well suited to monitor the sequence of the process, the time resolution

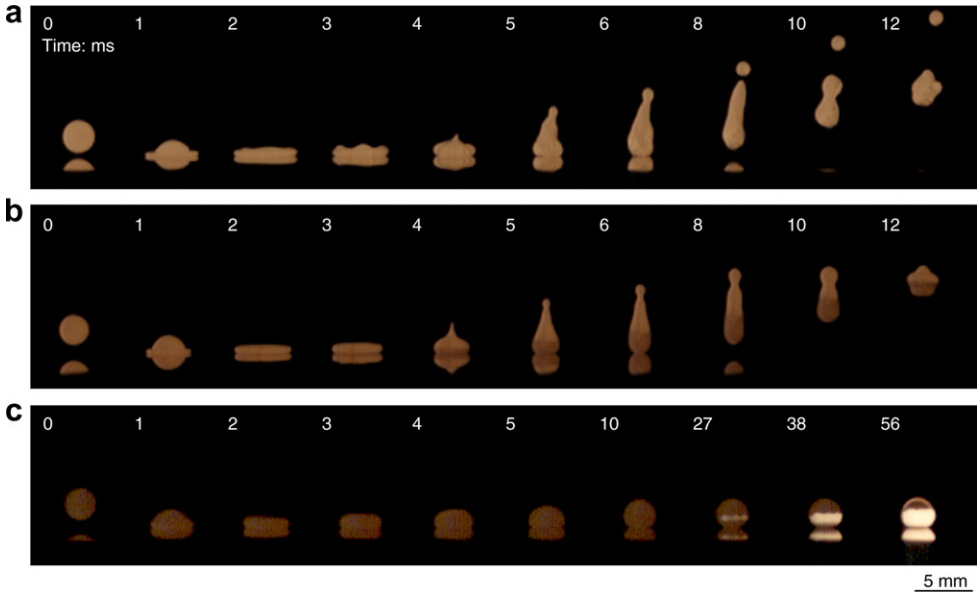

Fig. 2. HSV images (256 × 240 pixels) of the spreading and solidification behavior of YAG samples dropped at different initial temperatures: (a) 2474 K, (b) 2070 K ($\Delta T = 143$ K), and (c) 1418 K ($\Delta T = 795$ K). The time was indicated in the unit of ms at the upper left in each image and set at 0 ms for one frame before impact.

is too low to determine the maximum of the spreading factor. Therefore, the period from the impact to the rebound was remeasured with a spatial resolution of ~0.08 mm/pixel at 5 kHz. Fig. 3 shows the spreading factor as a function of time for the samples at various initial temperatures. The length of the spread droplet was measured at the maximum diameter, not at the droplet/substrate interface. The plateau shown at around $t = \sim 1.8$ ms suggests that the time resolution achieved at 5 kHz is sufficient for this analysis. The maximum spreading factor decreased with increasing initial undercoolings. Moreover, the time required to reach the maximum spreading factor also decreased. The time (t_C) taken for a droplet to spread to its maximum extent is predicted to be $8d/3v$ [6], where d is initial droplet diameter and v is the impact velocity. For the present experiment, t_C can be calculated as 3.9 ms, which is independent of the initial undercooling. It was not consistent with the present case.

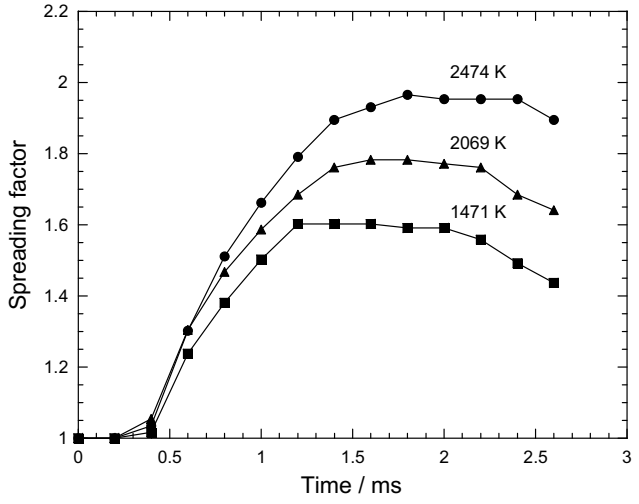

Fig. 3. Spreading factor of YAG samples as a function of time for the samples with different initial temperatures: (a) 2474 K, (b) 2069 K ($\Delta T = 144$ K), and (c) 1471 K ($\Delta T = 742$ K).

In order to reveal the effect of the wettability between the droplet and the copper substrate, the copper substrate was heated to different temperatures. The droplet temperature before release was kept at around the melting point. When the substrate temperature was lower than 423 K, rebound was observed. An attachment between the droplet and the substrate was found above 473 K since the improved wettability facilitated solidification. In the case of a substrate temperature higher than 573 K, the surface oxidation was detected. Therefore, the substrate temperature of 523 K was selected for further study.

For the copper substrate heated to 523 K, the spreading and solidification behavior were again observed using the HSV at 1 and 5 kHz, as shown in Fig. 4. The spreading behavior was very similar to the case of the copper substrate at room temperature. The main differences observed were the detachment processes of the small droplets, since the droplet attached to the substrate due to the improved wettability. In the sample dropped at 2271 K (a), many small droplets detached from the main droplet. Even at 1772 K ($\Delta T = 441$ K), a single small droplet detached and solidification was observed at ~10 ms, as shown by an arrow. Finally, in sample dropped at 1675 K ($\Delta T = 538$ K) (c), no detachment was observed and solidification started from the center, similarly to Fig. 2c.

Fig. 5 shows the maximum spreading factor determined by the HSV at 5 kHz as a function of initial droplet temperatures. The solid and open circles indicate the experimental results for the copper substrate at room temperature and

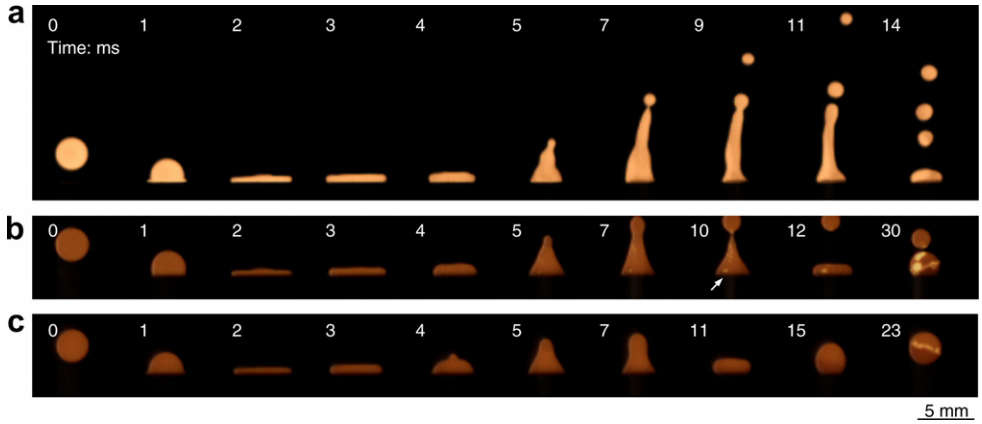

Fig. 4. HSV images of spreading and solidification behavior of YAG samples dropped on the 523 K copper substrate at different initial temperatures of (a) 2271 K, (b) 1772 K ($\Delta T = 441$ K), and (c) 1675 K ($\Delta T = 538$ K). The time was set at 0 ms for one frame before impact. The time was indicated in the unit of ms at the upper left in each image and set at 0 ms for one frame before impact.

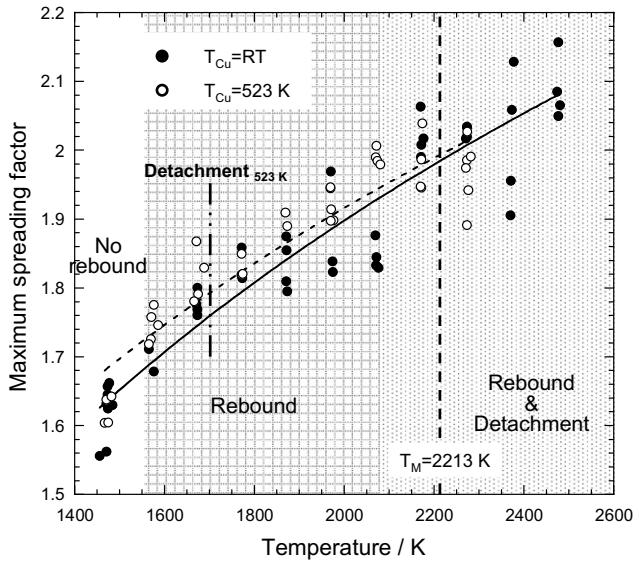

Fig. 5. Maximum spreading factor of YAG samples as a function of initial droplet temperatures. The solid and open circles indicate the experimental results for the copper substrate at room temperature and 523 K, respectively.

523 K, respectively. The measurement error in the spreading factor was roughly ±0.1 due to the low spatial resolution of the HSV at 5 kHz. The spreading factor monotonically decreased from ~2.1 to ~1.6 with decreasing initial droplet temperatures, which can be expressed by the fits

$$D_{MAX}/d = -4.605 + 1.97 \cdot \log(T)$$

for the substrate at room temperature (solid line), (1)

$$D_{MAX}/d = -3.873 + 1.75 \cdot \log(T)$$

for the substrate at 523 K (dotted line), (2)

where D_{MAX} is the maximum diameter and T is the droplet temperature. No difference in maximum spreading factor for the two kinds of substrate temperatures was found within the measurement error. In the case of conditions such as splashing, the substrate temperature is critical for predicting the spreading behavior [13]. The substrate temperature was not critical in terms of maximum spreading factor for the present case. In the case of the substrate at room temperature, the occurrence of "rebound and detachment" was observed until ~2100 K, while the droplets stopped rebounding at ~1550 K, as indicated by the hatchings. On the other hand, in the case of the substrate at 523 K, detachment was observed until ~1700 K, which is indicated by a double dotted line.

4. Discussion

The *in situ* observation of spreading and solidification of a YAG droplet was carried out using the separative ADL as a function of undercoolings. Before considering the spreading behavior, the difference in the droplet temperature between before release and before impact was discussed. The brightness of the levitated droplet during freefall as measured by the HSV was correlated to the pyrometric temperature. According to the correlation curve, the difference in the droplet temperature between before release and before impact decreased from ~220 K at 2273 K to ~90 K at 2073 K. The temperature of the droplet before its release was just assumed to be the same as that before impact, since the difference was negligible at the temperature lower than 2000 K.

The maximum spreading factor decreased from 2.1 to 1.6 with increasing undercoolings, as shown in Fig. 5. The maximum spreading factor has been derived by the energy conservation law, wherein the kinetic energy just before impact and the surface energy are converted into energy dissipation due to the viscosity and energy increase due to the enlarged surface area at the maximum spread diameter, as follows [14]:

$$\frac{D_{MAX}}{d} = \sqrt{\frac{We + 12}{3(1 - \cos\theta_a) + 4(We/\sqrt{Re})}}, \quad (3)$$

where We is Weber number ($\rho dv^2/\gamma$), Re is Reynolds number ($\rho dv/\eta$), and θ_a is the advancing liquid–solid contact angle. Moreover, ρ is density, γ is surface energy, and η is viscosity. The dominant factors contributing to the decrease in the maximum spreading factor are discussed using Eq. (3). The viscosity and the surface energy of the YAG above the melting point [15], and the density for a wide range of temperatures including the undercooled region [16] were determined experimentally as follows:

$$\eta = 1.48 \times 10^{-3} \cdot \exp\left(\frac{7714}{T}\right) \text{ Pa s} \quad (2243 \leqslant T/\text{K} \leqslant 2343)\ [15], \tag{4}$$

$$\gamma = 10^{-3} \cdot (850 - 0.035 \times T) \text{ N/m} \quad (2243 \leqslant T/\text{K} \leqslant 2343)\ [15], \tag{5}$$

$$\rho = 3.99 \times 10^3 - 0.29 \cdot (T - T_M) \text{ kg/m}^3 \quad (1470 \leqslant T/\text{K} \leqslant 2420)\ [16]. \tag{6}$$

θ_a increased roughly from 120° to 140° with decreasing temperature according to the HSV images. The temperature dependence of θ_a was roughly assumed to be linear because of the low spatial resolution of the HSV,

$$\theta_a = -0.01538 \cdot T + 158.45 \quad (1200 \leqslant T/\text{K} \leqslant 2500). \tag{7}$$

The physical properties shown above were used to calculate Eq. (3) by extrapolation to the undercooled region. The impact velocity, 1.7 m/s, and the initial diameter, 2.5×10^{-3} m, were also used. The experimental results of Eq. (1) and the calculation of Eq. (3) are plotted in Fig. 6a by solid circles and solid triangles, respectively. Although the calculation yields lower values than the experimental results for the low temperature range, the calculation well explains the spreading behavior of the YAG on the whole.

Here, the viscosity of the YAG in the undercooled region is empirically reported as $10^{1.5}$ Pa s at ~1600 K by the fiber-pulling experiment [17] and is known to be fragile, in comparison to the typical strong melt of SiO_2 [18]. Moreover, the glass transition temperature (T_g) is reported as 1154 K [19]. Therefore, the temperature dependence on viscosity was expressed by following the Vogel–Tammann–Fulcher equation, assuming that the viscosities at T_g, 1600 K and T_M are 10^{12}, $10^{1.5}$ and 0.048 Pa s, respectively:

$$\eta = 1.7 \times 10^{-6} \cdot \exp\left(\frac{14,500}{T - 800}\right) \text{ Pa s}. \tag{8}$$

Eq. (8) is plotted by solid squares in Fig. 6b. The extrapolation of Eq. (4) to the undercooled region is also plotted by solid triangles in Fig. 6b. It is evident that the viscosity in Eq. (8) increases more rapidly with decreasing undercoolings than it does in Eq. (4). The maximum spreading factor was again calculated by combining Eq. (8) with Eq. (3) and then plotted by solid squares in Fig. 6a. No agreement between the experimental results (solid circles) and the calculation (solid squares) was found for the whole temperature range. The spreading factor of $D_{MAX}/d < 1$, which cannot be defined, indicates that Eq. (3) is not applicable to the case of $Re < \sim 10$. This result suggests that the viscosity of the YAG at the undercooled region is considerably low even at 1400 K, and then increases rapidly to 10^{12} Pa s at T_g. This is consistent with the monotonic increase in growth velocity as a function of undercoolings [11] because the suppression of the atomic diffusion by increase in viscosity should result in decrease in the growth velocity.

The rebound of the droplets was observed until ~1550 K for the substrate at room temperature. Using

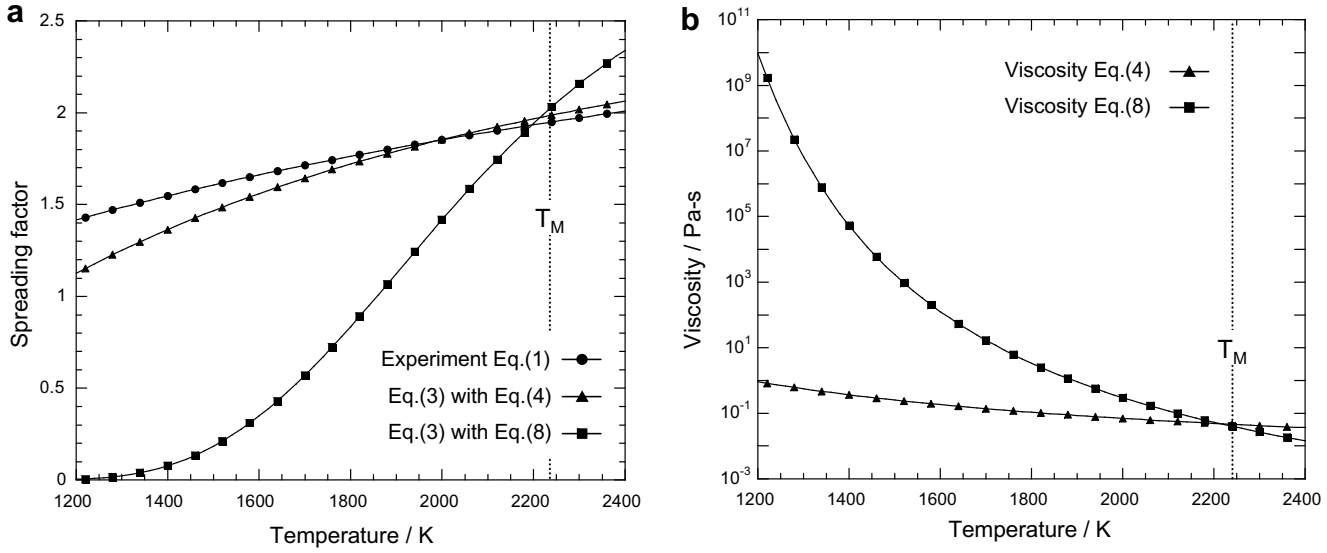

Fig. 6. (a) Maximum spreading factor as a function of initial droplet temperatures. Solid circles, triangles and squares indicate the fitted data (Eq. (1)) of experimental results, the calculation using Eq. (3) with Eq. (4) and the calculation using Eq. (3) with Eq. (8), respectively. (b) Viscosity as a function of initial droplet temperatures. Solid triangles and squares indicate viscosities calculated by Eqs. (4) and (8), respectively.

the energy conservation law, Mao et al. have derived the critical energy for the rebound as a function of the maximum spreading factor and the static contact angle [20]. It is difficult to measure the static contact angle of an undercooled droplet. Therefore, the relationship between the energy conservation in the system and undercooling is discussed by experimentally determining the total energies both before impact and at the rebound. The total energy before the impact can be given as $E^{in}_{Total} = E^{in}_{K} + E^{in}_{S}$ where E^{in}_{K} is the kinetic energy before impact and E^{in}_{S} is the surface energy of the droplet. The droplet spread into a thin disk with the lapse of time, kinetic energy reduced to zero at the maximum spread diameter due to both the viscosity dissipation and increase in the surface energy for enlarged surface area. Finally, a rebound takes place if the stored surface energy is greater than the viscosity dissipation during the recoil. Fig. 7a shows a schematic of the droplet impact, spread, rebound and second impact. Here, the droplet is largely stretched at the stage of the maximum recoil and vibrates once it bounces off, as shown in Fig. 2b. It is difficult to evaluate the vibration energy. Therefore, it was assumed that the shape of the droplet is a sphere just at the bounce (i.e. $E^{in}_{S} = E^{out}_{S}$) and that the upward velocity is the same as the downward velocity at the second impact.

Fig. 7b shows a semi-experimental map for contributed energies as a function of the initial droplet temperature. E^{in}_{K} and E^{out}_{K} were calculated using the velocities determined by the sequential HSV images of the first and second impacts, while E_S was calculated using Eq. (5). E_D is viscosity dissipation during spreading and recoiling. At temperatures above 2000 K, the detachment of a small droplet occurred as shown in Fig. 2a, which precludes accurately calculating the kinetic energy at the second impact accurately. E^{in}_{K} is constant because of the constant freefall distance of 15 cm, while E^{out}_{K} decreased with increasing undercoolings due to the viscosity dissipation and finally become zero at ~1600 K. When the Froude number ($Fr = v/(dg)^{1/2}$, g is gravity) is calculated as a function of the initial droplet temperature, Fr becomes unity at ~1600 K, indicating that the upward and downward velocities balanced each other at this temperature. It is noted that the downward velocity at the second impact was used in Fr, although Megaridis et al. used the downward velocity at the first impact in Fr to discuss the rebound behavior [21].

Finally, the surface energy and viscosity contributions to the decrease in the maximum spread factor and to the disappearance of the rebound with increasing undercoolings are considered. The disappearance of the rebound indicates that the stored surface energy was completely consumed by the viscosity dissipation just at the complete recoil. Re decreased from ~500 to ~20 with a temperature decrease from 2500 K to 1200 K, while the change of We was negligible, ~38. These results suggest that the main factor to controlling the system changed from surface energy to viscosity dissipation. Delplanque and Rangel also discussed this behavior wherein the energy contribution history was calculated with the lapse of time (see Fig. 6 [22]) and showed the transition from surface energy control to viscosity dissipation control, as depending on Re and We.

5. Conclusions

The combination of the separative ADL and the HSV elucidated the influence of undercoolings on the spreading and solidification for the YAG. The maximum spread factor decreased and the rebound disappeared with increasing undercoolings. The analysis based on the energy conservation law suggests that the main factor to control the system changed from surface energy to viscosity dissipation.

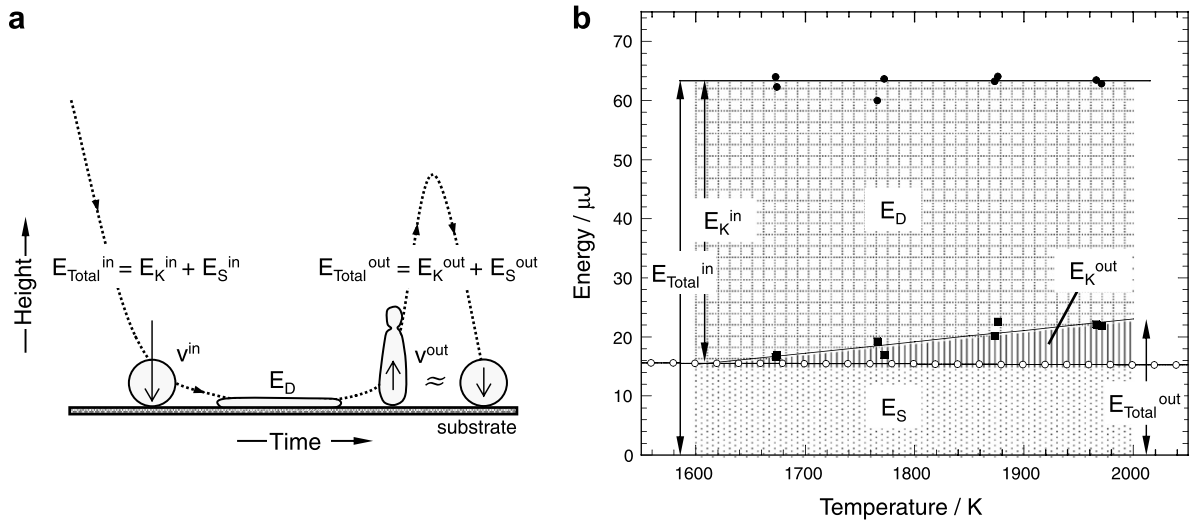

Fig. 7. (a) Schematic of droplet impact, spread, rebound and second impact. (b) Semi-experimental map for contributed energies as a function of initial droplet temperature.

Acknowledgement

This study was financially supported by a Grant-in-Aid for Scientific Research from the Ministry of Education, Culture, Sports, Science and Technology, Japan.

References

[1] N.P. Padture, M. Gell, E.H. Jordan, Thermal barrier coatings for gas-turbine engine application, Science 296 (2002) 280–284.
[2] M. Vardelle, A. Vardelle, P. Fauchais, C. Moreau, Pyrometer system for monitoring the particle impact on a substrate during a plasma spray process, Meas. Sci. Technol. 5 (1994) 205–212.
[3] P. Gougeon, C. Moreau, Simultaneous independent measurement of splat diameter and cooling time during impact on a substrate of plasma sprayed molybdenum particles, J. Therm. Spray Technol. 10 (2001) 76–82.
[4] K. Shinoda, Y. Kojima, T. Yoshida, In situ measurement system for deformation and solidification phenomena of yttria-stabilized zirconia droplets impinging on quartz glass substrate under plasma spraying conditions, J. Therm. Spray Technol. 14 (2005) 511–517.
[5] P.S. Grant, B. Cantor, L. Katgerman, Acta Metal. Mater. 41 (1993) 3097.
[6] M. Pasandideh-Fard, R. Bhola, S. Chandra, J. Mostaghimi, Deposition of tin droplets on a steel plate: simulations and experiments, Int. J. Heat Mass Transfer 41 (1998) 2929–2945.
[7] P. Fauchais, M. Fukumoto, A. Vardelle, M. Vardelle, Knowledge concerning splat formation: an invited review, J. Therm. Spray Technol. 13 (2004) 337–360.
[8] K. Nagashio, M. Adachi, K. Higuchi, A. Mizuno, M. Watanabe, K. Kuribayashi, Y. Katayama, Real time X-ray observation of solidification from undercooled Si melt, J. Appl. Phys. 100 (2006) 033524.
[9] K. Nagashio, H. Murata, K. Kuribayashi, In situ observation of solidification behavior of Si melt dropped on Si wafer by IR thermography, J. Cryst. Growth 275 (2005) e1685–e1690.
[10] K. Nagashio, H. Murata, K. Kuribayashi, Spreading and solidification behavior of molten Si droplets on substrates, Acta Mater. 52 (2004) 5295–5301.
[11] K. Nagashio, K. Kuribayashi, Rapid solidification of $Y_3Al_5O_{12}$ garnet from hypercooled melt, Acta Mater. 49 (2001) 1947–1955.
[12] K. Nagashio, K. Kuribayashi, O. Yamaguchi, T. Hibiya, In situ observation of formation of metastable rare-earth iron garnet by splat quenching, J. Am. Ceram. Soc. 90 (2007) 238–243.
[13] M. Fukumoto, S. Kato, M. Ohwatari, Y. Huang, Splatting and solidification behavior of plasma sprayed metallic powders impinging on flat SUS304 substrate, J. Jpn. Inst. Metals 59 (1995) 1178 (in Japanese).
[14] M. Pasandideh-Fard, Y.M. Qiao, S. Chandra, J. Mostaghimi, Capillary effects during droplet impact on a solid surface, Phys. Fluids 8 (1996) 650.
[15] V.J. Fratello, C.D. Brandle, Physical properties of a $Y_3Al_5O_{12}$ melt, J. Cryst. Growth 128 (1993) 1006.
[16] P.-F. Paradis, J. Yu, T. Ishikawa, T. Aoyama, S. Yoda, J.K.R. Weber, Contactless density measurement of superheated and undercooled liquid $Y_3Al_5O_{12}$, J. Cryst. Growth 249 (2003) 523.
[17] J.K.R. Weber, J.J. Felten, B. Cho, P.C. Nordine, Glass fibers of pure and erbium- or neodymium-doped yttria–alumina compositions, Nature 393 (1998) 769.
[18] C.A. Angell, Formation of glasses from liquids and biopolymers, Science 267 (1995) 1924.
[19] K. Nagashio, K. Kuribayashi, Spherical yttrium aluminum garnet embedded in a glass matrix, J. Am. Ceram. Soc. 85 (2002) 2353.
[20] T. Mao, D.C.S. Kuhn, H. Tran, Spread and rebound of liquid droplets upon impact on flat surfaces, AIChE J. 43 (1997) 2169.
[21] C.M. Megaridis, K. Boomsma, I.S. Bayer, Partial rebound of molten-metal droplets impacting on solid substrates, AIChE J. 50 (2004) 1356.
[22] J.-P. Delplanque, R.H. Rangel, An improved model for droplet solidification on a flat surface, J. Mater. Sci. 32 (1997) 1519.